Using sub-pixel roughness estimates from ASTER stereo images to compensate for roughness effects in the thermal infrared

A. Mushkin[1*], A. R. Gillespie[1], I. Danilina[1], M. O'Neal[2], L. Pietro[2], E. Abbott[3], L. Balick[4].
[1]*University of Washington, Seattle WA 98195*
[2]*University of Delaware, Newark DE 19716*
[3]*Jet Propulsion Laboratory, Pasadena CA 91109*
[4]*Los Alamos National Laboratory, Los Alamos NM 87545*
* mushkin@u.washington.edu

ABSTRACT- *Sub-pixel roughness affects remote thermal infrared (TIR) data through two main processes: shadowing, which leads to temperature gradients within the pixel, and cavity radiation, which decreases the apparent spectral contrast in the TIR. To compensate for these effects we suggest an integrated approach that combines remote roughness measurements from ASTER (Advanced Spaceborne Thermal Emission and Reflection Radiometer) stereo images with a TIR radiosity model. We used high-resolution (~5 mm) DEM's (HR-DEM's) of natural bare surfaces, measured with a ground-based laser scanner, to calibrate relative ASTER stereo roughness estimates against RMS roughness measured directly from the HR-DEM's. The HR-DEM's were input to a radiosity model, which enables quantification of the increase in surface-leaving TIR radiance from multiple scattering in cavities, and thus calculation of roughness-dependent transformation functions between the emissivity of smooth surfaces, as measured in the lab, and the effective emissivity of rough natural surfaces of the same composition. Numerical simulations suggest that the ±5% accuracy assumed for the ASTER stereo RMS roughness estimates would be sufficient to compensate for cavity radiation effects on ASTER TIR emissivity retrievals from rough isothermal surfaces with RMS < 0.13 m. The main challenges in the way of applying these corrections to actual TIR ASTER image data are measuring the 3D roughness of various terrain types with RMS > 0.13 m, and adjusting the TIR radiosity model to account for differential solar heating due to shadowing.*

1 INTRODUCTION

The unresolved topographic expression of the surface at sub-pixel scales (surface roughness) is a key parameter for many geological, hydrological and planetary studies, as well as an essential variable for a wide range of remote-sensing applications across the electro-magnetic spectrum. Surface roughness affects thermal infrared (TIR) imaging of natural surfaces mainly through two physical processes: 1) shadowing, which creates surface temperature (T) gradients within the pixel, and 2) 'cavity radiation' from multiple reflections between roughness elements. Both processes affect T and emissivity (ε) retrievals from remote TIR measurements. In this regard, compensation for super-pixel topography effects can be achieved with digital elevation models (DEM's) combined with radiosity models, but correction for sub-pixel surface roughness effects can only be addressed implicitly, and requires statistical estimates of surface roughness at sub-pixel scales.

In this study we present a new method to quantify sub-pixel surface roughness from remote-sensing data, which is generally applicable with stereoscopic or repeat image data, in terrestrial (Mushkin and Gillespie, 2005) as well as planetary environments (Mushkin and Gillespie, 2006). Here, we focus on its application using ASTER (Advanced Spaceborne Thermal Emission and Reflection Radiometer; Yamaguchi et al., 1998) stereoscopic image data, and also discuss the basis of a new approach to compensate for surface roughness effects on ε retrievals using the ASTER T/ε separation algorithm of Gillespie et al. (1998).

2 APPROACH AND METHODOLOGY

2.1 Relative roughness using ASTER

Natural rough surfaces in the visible wavelengths are typically darkened by shadows. Quantifying the amount of shadows on the surface from remote-sensing data is not a trivial task because it requires separating

the non-correlated effects of albedo (i.e., surface composition) and unresolved, sub-pixel shadows. For bare surfaces, this problem can be addressed using the ratio between co-registered stereo images. Deviation from a value of unity for this ratio primarily reflects the difference between the effective fraction of unresolved shadows in the pixel, as 'seen' by the sensor from the two view angles (Fig. 1). In the case of non-structured surfaces and no compositional changes on the ground between the two measurements, this ratio can be used as a proxy for relative sub-pixel roughness variations, which is independent of surface composition (Mushkin and Gillespie, 2005 for details).

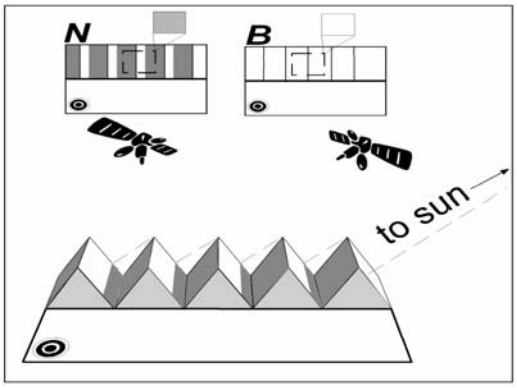

Figure 1: *Illustration of the stereoscopic approach for estimating sub-pixel surface roughness. A pixel in the rough section of the surface viewed from nadir (N) will have a lower DN value than the same pixel viewed down-sun (B), where shadows become hidden behind sunlit surface elements. DN values for pixels in a smooth Lambertian surface will not change with view angle because there are no shadows. Accordingly, the ratio between DN values of corresponding pixels can be used as a proxy for sub-pixel surface roughness.*

The ASTER sensor on-board 'Terra' is especially suited for application of this 'two-look' approach because of its stereoscopic imaging capability made possible by an additional channel (3B) of 15 m data that is acquired at the same wavelengths and spatial resolution as the nadir channel at ~0.81 μm (3N), but ~55 seconds later and looking back 27.6° from nadir. Although 3B data were primarily designed for independent generation of ~30-m DEM's, which are available as a validated standard ASTER product, unregistered channel 3B data are included with ASTER Level-1B daytime data. Hence, a simple ratio between co-registered ASTER 3B and 3N images yields an image of relative sub-pixel roughness variations within a given scene (Fig. 2).

The number of separable roughness levels that can be derived using this approach strongly depends on solar elevation, which determines the length of shadows and the magnitude of lightness differences between the two looks (Fig. 1). For solar elevations that exceed ~60° above horizon, ASTER 3B over 3N ratio image becomes dominated by sensor noise.

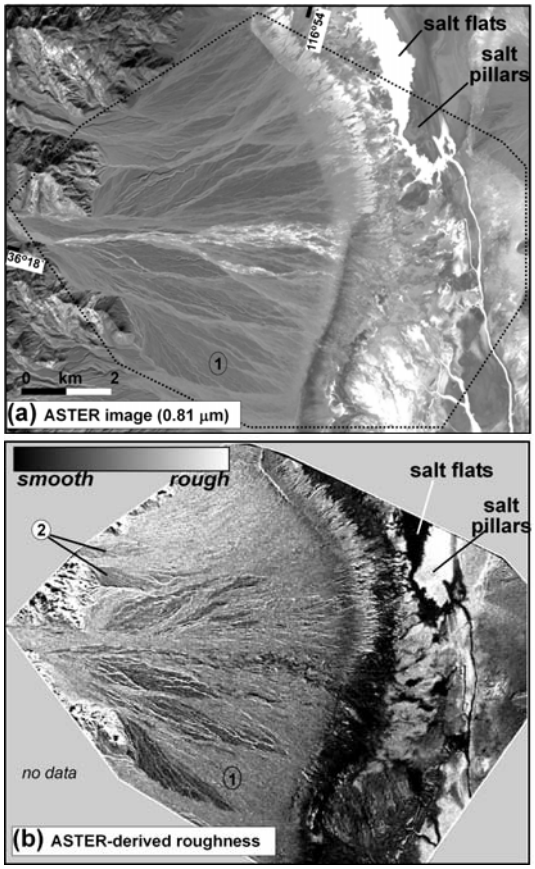

Figure 2: *Relative sub-pixel roughness estimates derived from ASTER data (15 m/pixel).* ***a****) ASTER channel 3N image of Trail Canyon fan, California USA.* ***b****) Ratio image between ASTER 3B and 3N channels as a proxy for sub-pixel surface roughness. Data acquired November 12th 2000, with solar elevation of 35°. Location 1 – in 2a this alluvial surface is only subtly darker than the adjacent surface to the west, which was observed in the field to be older and smoother. In 2b they are clearly distinguished. The light salt flats and the adjacent dark salt-pillar terrain in 2a are correctly identified as smooth and rough, respectively, in 2b.*

In most cases atmospheric corrections are not required for ASTER relative roughness estimates because 1) the ratio between atmospheric transmissivities in channels 3B and 3N can be regarded as constant multiplicative factor across the scene and thus a linear scaling factor for the relative roughness estimations, and 2) in the case that path radiance << total measured signal, the ratio between un-compensated measurements may not be equal, but is proportional to the ratio of calibrated reflectance data. Yet, applying a path-radiance correction (e.g., 'dark-object subtraction') can improve the contrast in the ASTER 3B over 3N ratio image and the number of separable roughness levels that can be derived.

2.2 Calibration

ASTER stereo roughness images (Fig. 2) require additional calibration for retrieval of 'absolute' quantitative roughness parameters. Such calibration can be achieved through a) empirical calibration in cases where independent in-situ roughness measurements of are available for a given study site (Mushkin and Gillespie, 2006) or b) more general model-based calibrations as presented in this study. In the latter calibration scheme we use hyper-resolution (~5 mm) DEM's (HR-DEM's) of natural bare surfaces and a single-scatter model to simulate the 3B to 3N ratio under the illumination geometry in the ASTER scene being used. The simulated ratios are then used to construct a scene-specific calibration curve that facilitates translation of the ASTER stereo ratio values to quantitative 'absolute' roughness parameters directly derived from the HR-DEM's.

Self-affine, synthetic model-surfaces are commonly used to describe the roughness of natural surfaces at sub-pixel scales. However, because natural surfaces are more complex, with multiple physical processes rather than a single one determining their micro-topographic expression (e.g., rock fragmentation, fine-particle accumulation, erosion), a fractal representation of sub-pixel roughness may be problematic (e.g., Weeks et al., 1996). Direct measurement of real surfaces may yield a more realistic description.

Ground-based laser scanners now enable 3D characterization of natural surfaces at very high resolutions, down to ~mm scales (Fig. 3), though it requires multiple measurements from different angles to overcome the problem of hidden areas behind roughness elements at the grazing view angles of a ground-based system. For this study we used a commercial Trimble GS200 3D scanner to measure the roughness of natural bare surfaces displaying a range of roughnesses in eastern California (Fig. 3).

To simulate ASTER 3B/3N ratio for these surfaces we use a single-scatter reflection model that assumes Lambertian reflection from the individual, mm-scale surface elements. The model accounts for shading, shadowing and the visibility of each surface element from ASTER 3B and 3N view angles. Key illumination geometry variables considered in the model are: terrain slope, solar elevation and angle between the solar principle plane and the satellite track.

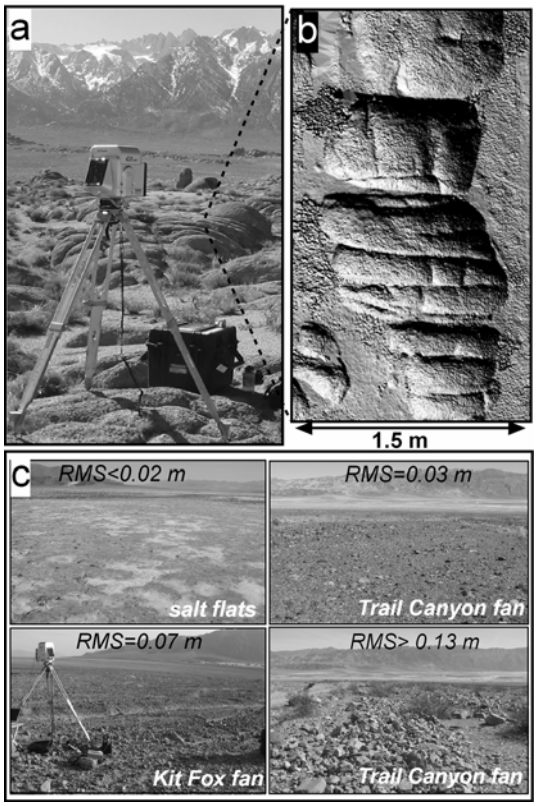

Figure 3: a) *LiDAR scanner in granite bedrock terrain, Albama Hills, California.* ***b)*** *A shaded relief image of a ~mm-scale DEM of the granite outcrop marked in (a). C) Surfaces used for calibration, Death Valley, California.*

Model-based 3B/3N predictions have to be compared to radiometrically calibrated and atmospherically corrected ASTER data. We remove the additive atmospheric path radiance term using a standard 'dark-object' subtraction and use MODTRAN (Ontar, 2001) standard model atmospheres to determine atmospheric transmisivities for both ASTER look-angles, because 3B data are not provided in the standard ASTER land-leaving radiance

product. A sensitivity analysis (not shown here) suggests that the maximum error introduced from these MODTRAN corrections, i.e., using the driest atmosphere coefficients to correct the wettest model atmosphere, is on the order of ~2%, and that use of ancillary information such as geographic location and acquisition time can reduce this error.

3 RESULTS

Figure 4a displays calculated calibration curves for different illumination geometries using the HR-DEM's from Death Valley, California.

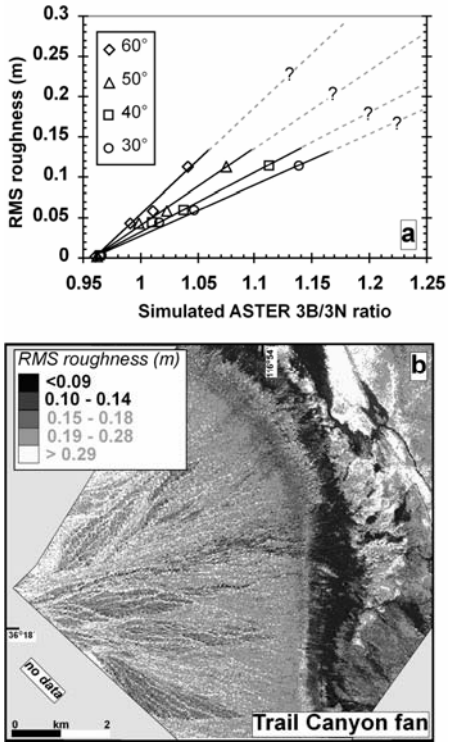

Figure 6: *Calibration to RMS roughness values.* ***a)*** *Calibration curves representing four different cases of solar elevations.* ***b)*** *ASTER 3B/3N ratio image calibrated to RMS roughness using the 50° calibration curve in (a). Dashed gray lines in (a) represent unconstrained extrapolation of the linear regressions, and thus RMS values above 0.13 m (in gray) are uncertain.*

The simulations suggest that a linear regression between surface RMS and ASTER 3B over 3N ratio is adequate for the range of measured RMS roughnesses, i.e., <~0.13 m. The slope of the regression is proportional to solar elevation, implying decreased separability between roughness levels as solar elevation increases. The 50° solar elevation regression in Figure 6a was used to translate an ASTER 3B/3N ratio image from October 1st 2000 into a quantitative surface RMS image (Fig. 6b) of Trail Canyon fan in Death Valley. Errors for the ASTER 3B/3N ratio are estimated as <1.5% and errors in the HR-DEM measurements are ignored. Compensation for atmospheric transmissivity was calculated using the '1976 Standard Atmosphere' model in MODTRAN. Estimated RMS values were binned into 5 classes, accounting for up to 5% error associated with system noise, image-to-image registration, atmospheric corrections and local variations in surface slope.

4 DISCUSSION

4.1 Roughness calibration

HR-DEM's enable calibration of relative stereo roughness estimation into 'absolute' roughness parameters, e.g., surface RMS (Fig. 6). Moreover, with such data, corrections for general terrain slopes, i.e., slopes at the scales of 'conventional' DEM's, can also be applied by mathematically adjusting the HR-DEM's in the reflection model. HR-DEM calibration is terrain-specific and should be applied carefully. For example, a calibration curve calculated for alluvial surfaces may not be appropriate for bedrock surfaces because these two surface types have a distinctly different organization, and regression coefficients describing the relation between the 3B/3N ratio and surface roughness may be different. Establishing a library of HR-DEM's for a wide variety of terrain types (e.g., alluvial surfaces; playa deposits, bedrock surfaces, planetary analogs) is now in progress. Additional aspects of this approach that require further study are the effect of vegetation on roughness estimations and improving the characterization of the rougher surfaces (RMS > ~0.13m), for which the present HR-DEM's are not adequate.

4.2 Compensation for surface roughness effects on ASTER emissivity retrievals

Surface roughness is directly related to two physical processes that affect remote TIR measurements of natural surfaces: 1) cavity radiation, which leads to increased surface-leaving radiation due to multiple scattering and 2) shadowing, which leads to temperature gradients within the pixel. The magnitude of these two separate processes is demonstrated in Figure 5 with ~8 K difference between cobble tops and 'warm halos' at their base shortly after sunset, and ~25 K difference between shadowed and sunlit scene elements shortly after noon on a sunny day. Here, we

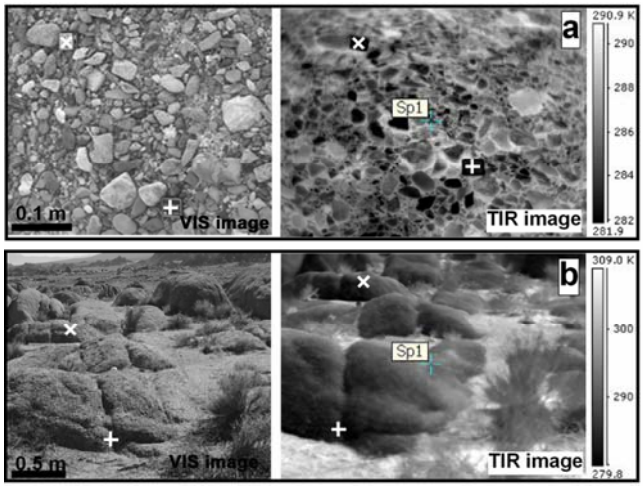

Figure 5: *Roughness effects in the TIR.* ***a)*** *FLIR image of alluvial gravels taken shortly after sunset near Owens Lake, California. The 'warm' regions around the individual clasts are due to cavity radiation.* ***b)*** *FLIR image of a granite bedrock outcrop acquired at 12:30 pm, Alabama Hills, California. In both cases, '+' and 'x' are co-registered with the overlapping VIS images to the left (taken from at slightly different view angles). Cavity radiation amounts to ~8 K difference, whereas shadow-sunlit differences are ~25 K. Note the complicating factor of low-thermal inertia gruss surfaces, which comprise the warmest elements in (b).*

discuss how these processes affect T and ε retrievals using the ASTER T/ε separation (TES) algorithm (Gillespie et al., 1998), and note that the magnitude of roughness effects depends on the T/ε separation algorithm being used.

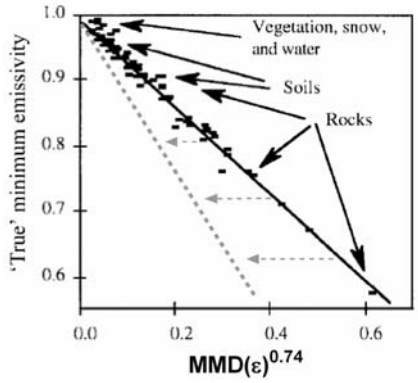

Figure 6: *ASTER TES MMD-ε_{min} regression. Solid black line is the Gillespie et al. (1998) regression derived from library emissivity spectra. Gray dashed line represents the shift expected when using emittance values to calculate the MMD. An upwards shift in ε_{min} estimates require a downward shift in T estimates.*

ASTER TES relies on the fact that an error in the assumed maximum ε may shift the values of apparent emissivities, but does not significantly change their spectral shape in the 8-12 μm region. An empirical regression (Fig. 6) is then used to relate the maximum-minimum spectral contrast of the apparent emissivities, (MMD) to the 'true' minimum emissivity (ε_{min}), which is then used to rescale the remaining apparent ε's and recalculate T. Therefore, in the range of typical temperatures on Earth, 270-330 K, ASTER TES ε retrievals are not expected to be significantly affected by sub-pixel temperature gradients, because in this case spectral shape is constant. In contrast, cavity radiation effectively reduces spectral contrast and affects both T and ε retrievals from TES. The MMD vs. ε_{min} regression is defined for laboratory emissivity measurements. Yet, the MMD derived from real image data is in fact for emittance (ε_m) values, defined here as effective emissivity of a rough surface. Because MMD(ε_m) < MMD(ε) due to cavity radiation, estimated ε_{min} values regressed from MMD(ε_m) are shifted upwards (Fig. 6) and T estimates are consequently shifted downwards. To correct for this effect a transformation between ε_m and ε values is required.

In a companion paper, Danilina et al. (this issue) use a TIR radiosity model to demonstrate that the magnitude of cavity radiation from an isothermal surface is correlated with its roughness through a logarithmic function (Fig. 7a). Their model also allows us to determine the slope of the linear transformation function between ε_m and ε for a given surface RMS (Fig. 7b). Thus, independent estimations of surface RMS from ASTER stereo data can be used to determine the appropriate transformation function to be used for translating MMD(ε_m) to MMD(ε), and thus compensating for the effects of cavity radiation on ASTER TES ε retrievals from isothermal surfaces (Fig. 8). However, application of such corrections to actual image data requires incorporation of temperature gradients into the TIR radiosity model, which are expected to decrease the effect of day-time cavity radiation as cavities are preferentially shadowed. Cavity effects may be enhanced for night-time data in which cavities may be warmer than their surroundings.

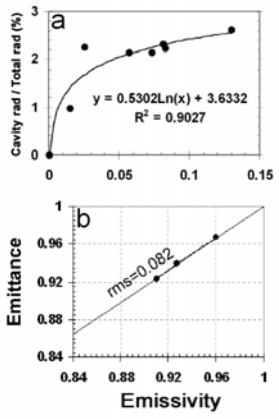

Figure 7: *Results from TIR radiosity model of Danilina et al. (this issue).* ***a)*** *Cavity radiation increase with surface roughness.* ***b)*** *The relation between emissivity and emittance determined from model results. The slope of this linear relation differs with surface roughness.*

5 SUMMARY

ASTER stereo image data can be used to obtain relative sub-pixel (~15 m) roughness estimates at solar elevation below 55° above horizon. These roughness estimates can be calibrated into quantitative roughness parameters using hyper-resolution (~5 mm) DEM's of real surfaces and a surface-reflection model that can account for the scene-specific illumination and viewing geometries. We use a TIR radiosity model for the same surfaces to determine the roughness-dependent transformation functions required to translate emittance values of rough surfaces to laboratory-measured emissivity values of smooth samples. In concert, ASTER stereo roughness measurements and the emittance-emissiviy transformation functions can be used to compensate ASTER TES ε retrievals for the effects of cavity radiation.

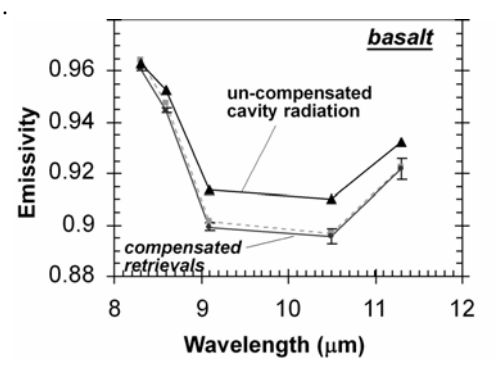

Figure 8: *Numerical simulations of compensation for cavity radiation effects on ASTER TES emissivity retrievals for a basalt surface with RMS=0.082 m. Gray dashed line represents library emissivities used. Error bars are 1-σ values arising from an introduced 5% random error in roughness estimations.*

ACKNOWLEDGEMENTS

We thank J. Macey for his help in the field and G. Yamada for her help in the processing of ASTER stereo data. Funding for this study was from NASA project NN604H255C (ASTER), the U. S. Department of Energy, Office of Nonproliferation Technology Development contract W-7405-ENG-36 and contract DE-AC52-06NA25396 to Los Alamos National Security, LLC. project, Los Alamos National Lab subcontract to the University of Washington and University of Washington student grants to AM and ID.

REFERENCES

Gillespie, A.R., Rokugawa, S., Matsunaga, T., Cothern, J.S., Hook, S., and Kahle, A.B., 1998, A Temperature and Emissivity Separation Algorithm for Advanced Spaceborne Thermal Emission and Reflection Radiometer (ASTER) Images: *IEEE Transcations on Geoscince and Remote Sensing*, v. 36(4), p. 1113-1126.

Mushkin, A., and Gillespie, A.R., 2005, Estimating sub-pixel surface roughness using remotely sensed stereoscopic data: *Remote Sensing of Environment*, v. 99, p. 75-83.

Mushkin, A., and Gillespie, A.R., in-press, Measuring sub-pixel Surface Roughness using High-Resolution Image Data: *Geophysical Research Letters*.

Ontar, 2001, PcModWin v 4.0: North Andover, MA 01845, USA.

Weeks, R.J., Smith, M.O., Pak, K., Li, W.-H., Gillespie, A.R., and Gustafson, W., 1996, Surface roughness, radar backscatter, and visible and near-infrared reflectance in Death Valley, California: *Journal of Geophysical Research*, v. 101(E10), p. 23,077-23,090.

Yamaguchi, Y., Kahle, A.B., Tsu, H., Kawakami, H., and Pniel, M., 1998, Overview of Advanced Spaceborne Thermal Emission and Reflection radiometer (ASTER): *IEEE Transactions on Geoscience and Remote Sensing*, v. 36(4), p. 1062-1071.